Seismic performance of a load-bearing prefabricated composite wall panel structure for residential construction

Journal:	*Advances in Structural Engineering*
Manuscript ID	ASE-19-0787.R1
Manuscript Type:	Original Research
Date Submitted by the Author:	11-Feb-2020
Complete List of Authors:	Huang, Qunyi; Southwest Jiaotong University, School of Civil Engineering Orr, John; University of Cambridge, Department of Engineering Huang, Yanxia; Anyang Institute of Technology, School of Civil and Architectural Engineering Xiong, Feng; Sichuan University, College of Architecture & Environment; Sichuan University, MOE Key Laboratory of Deep Underground Science and Engineering Jia, Hongyu; Southwest Jiaotong University, School of Civil Engineering
Keywords:	Prefabrication, Composite panels, Quasi-static testing, Seismic performance, Residential construction
Abstract:	To improve both seismic performance and thermal insulation of low-rise housing in rural areas of China, the present study proposes a new type of building structure that achieves appropriate seismic performance and energy efficiency using field-assembled load-bearing prefabricated composite wall panels (LPCP). A 1:2 scale prototype built using LPCP is subjected to quasi-static testing so as to obtain damage characteristics, load-bearing capacity, and load-displacement curves in response to a simulated earthquake. As a result, seismic performance indicators of load-bearing capacity, deformation, and energy-dissipating characteristics, are assessed against the corresponding seismic design requirements for rural building structures of China. Experimental results indicate that the earthquake-resistant capacity of the prototype is 68% higher than the design value. The sample has a ductility factor of 4.7, which meets the seismic performance requirement mandating that the ductility factor of such concrete structures should exceed 3. The design can be further optimized to save the consumption of material. This shows that the LPCP structure developed here has decent load-bearing capacity, ductility and energy dissipation abilities, a combination of which is in line with the earth quake specifications. A new construction process proposed here based on factory prefabrication and field assembly leads to a considerable reduction of energy consumption.

Seismic performance of a load-bearing prefabricated composite wall panel structure for residential construction

QunyiHuang[a,b], John Orr[c], YanxiaHuang[d,*], Feng Xiong[b],HongyuJia[a]

Abstract

To improve both seismic performance and thermal insulation of low-rise housing in rural areas of China, the present study proposes a new type of building structure that achieves appropriate seismic performance and energy efficiency using field-assembled load-bearing prefabricated composite wall panels (LPCP). A 1:2 scale prototype built using LPCP is subjected to quasi-static testing so as to obtain damage characteristics, load-bearing capacity, and load-displacement curves in response to a simulated earthquake. As a result, seismic performance indicators of load-bearing capacity, deformation, and energy-dissipating characteristics, are assessed against the corresponding seismic design requirements for rural building structures of China. Experimental results indicate that the earthquake-resistant capacity of the prototype is 68% higher than the design value. The sample has a ductility factor of 4.7, which meets the seismic performance requirement mandating that the ductility factor of such concrete structures should exceed 3. The design can be further optimized to save the consumption of material. This shows that the LPCP structure developed here has decent load-bearing capacity, ductility and energy dissipation abilities, a combination of which is in line with the earth quake specifications. A new construction process proposed here based on factory prefabrication and field assembly leads to a considerable reduction of energy consumption.

Key words： Prefabrication; Composite panels; Quasi-static testing; Seismic performance; Residential construction

[1]School of Civil Engineering, Southwest Jiaotong University, Chengdu, China;

[2]College of Architecture and Environment, Sichuan University, Chengdu, China;

[3]Department of Engineering, University of Cambridge, Trumpington Street, Cambridge, UK;

[4]School of Civil and Architectural Engineering, Anyang institute of Technology, Anyang, China

Corresponding author

Yanxia Huang, School of Civil and Architectural Engineering, Anyang institute of Technology,West section of Huanghe Avenue, Anyang 45000, China

Email: huangyanxia0301@hotmail.com

1. Introduction

Located between the circum-Pacific earthquake zone and the Euro-Asian earthquake zone, China is one of the most earthquake-prone countries in the world. A review of historical data reveals that earthquakes in China are mostly characterized by high frequency, shallow hypocentres, great intensity, and wide distribution(Huang et al,2014; Jia et al 2013).Since the Tang Shan earthquake in 1976, a multitude of destructive earthquakes took place in China, with the majority of which occurring in broad and densely populated rural areas(Tian et al, 2006). Most rural building structures in China are self-built, primarily in masonry, brick, or wood, and often exhibit poor seismic performance. During the 2008 Great Wenchuan earthquake (8.0 Ms), such rural buildings were subject to severe damage or even total collapse.

The sintering of clay to make solid bricks for rural buildings consumes large amount of coal, with associated CO2 emissions, and the manufacturing process emits significant amount of dust, which can lead to severe environmental pollution(Cao et al, 2015). According to Ji(2018), 1770-2077kg of coal are needed to produce 10,000 solid bricks in China. Such issues are barriers to the promotion of energy conservation technology in rural building structures. Therefore, there exists an urgent need to develop an integrated technology that can simultaneously enhance the seismic performance and energy efficiency of rural building structures.

To enhance the seismic performance and energy efficiency of rural building structure, this paper details the development of the Load-bearing Prefabricated Composite wall Panel (LPCP) to serve as the primary load-bearing and thermal insulation component for establishing the rural building structure with appropriate seismic performance and energy efficiency based on factory prefabrication and field assembly. The proposed LPCP is a sandwich construction, with a central thermal insulation layer enclosed between two steel mesh reinforced concrete layers.

The reinforced concrete layers are connected through an array of two-way diagonal reinforcing bars so as to form a steel-mesh-reinforced concrete composite plate (Fig. 1). The insulation thickness can be adjusted in accordance with the regional climate condition and energy efficiency requirements. The strength, spacing and diameter of the reinforcing bars in the reinforcement mesh as well as the strength and thickness of the concrete layers is determined based on structural calculations.

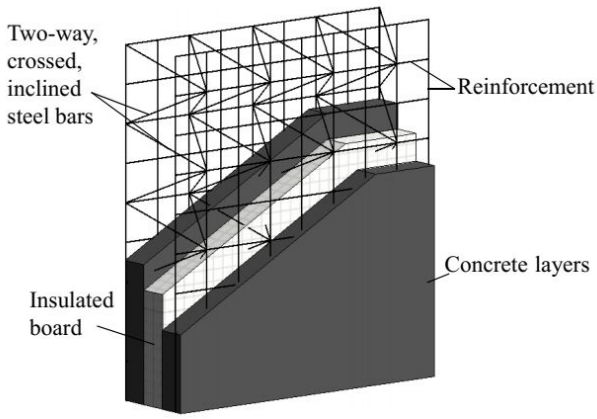

Figure 1. Schematic of load-bearing prefabricated composite wall panel

Wang(2016)examined the statistical data of China Real Estate Evaluation Centre concerning the difference of reinforced-concrete structure constructions between industrial method and the traditional cast-in-place concrete construction method. It was found that the former method reduces the energy consumption by 20% ~ 30%, material loss by 60%, construction rubbish by 83%, and recyclable materials by 66% compared to the latter method, a combination of which eventually leads to the reduction of carbon emission. Thus, it is advised to construct LPCP building by the industrial method based on in-factory prefabrication and field assembly of the construction parts, which not only delivers the advantage of reinforced-concrete structure, but can also reduce the energy consumption and carbon emission, making this new structure particularly promising.

Research indicates that this type of sandwich plate exhibits good load bearing capacity and ductility with the presence of axial vertical load (Rodrigo et al, 2013; Mohamad et al, 2013; Benayoune et al, 2007), eccentric vertical load (Mohamad et al, 2011; Benayoune et al, 2006), bending (Isabella et al, 2015; Smitha et al, 2014; Ramachandra et al, 2014; Benayoune et al, 2008), shear force (Liu et al, 2013;Waiel et al, 2009; Wu et al, 2006), compressive-bending-shear composite load (Kabir, 2005), and seismic load (Janardhana et al,2014; Magliulo et al, 2014; Retamales et al, 2013), making it suitable to be used as the main load-bearing component in multi-story building structures. This conclusion provided an idea that the LPCP, a kind of seismic resistance and energy saving prefabricated sandwich wall panel, also could be applied in the multi-storey buildings to improve the seismic resistance in rural area of China. Thus, Huang et al(Huang et al, 2014, 2018) investigated the seismic performance of the LPCP by testing and numerical simulation. The results indicated that the seismic performance indexes such as bearing capacity, deformation capacity and energy dissipation capacity can meet the corresponding seismic fortification requirements. However, LPCP is a kind of prefabricated component, which needs to be transported to the site for assembly to form a structure. Connections method between components, components and foundations, and whether the aseismic performance indicators of the assembled structure can meet the requirements of aseismic fortification still needs further research.

To address this gap in the knowledge, this paper details the design, construction, and testing of a 1:2 scale model of an LPCP building structure. Quasi-static testing was undertaken to obtain damage characteristics, yield load, and load-displacement curves of the building structure in response to the simulated seismic conditions. This work allows us to determine whether a suite of seismic performance indicators, e.g., load-bearing capacity, ductility, and

energy-dissipating ability, can meet the seismic performance requirements of rural building structure.

2. LPCP Prototype Testing

2.1 *Reference building*

The specimen is prototyped based on a rural building in the City of Leshan in China's Sichuan Province. This reference building is 13.2 m tall and has a storey height of 3.3 m. The standard floor layout and the cross-section plot of the building are shown in Fig. 2. The Seismic Precautionary Intensity is set to 7 according to the code for design of buildings of China (2010). Here the Seismic Precautionary Intensity refers to the seismic intensity prescribed by the national regulation for benchmarking the seismic performance of buildings in the local area. It is calculated as the seismic intensity the local area has more than 10% likelihood to experience within five decades. The seismic intensity refers to the extent to which the ground and buildings are damaged during an earthquake. The level 7 of Seismic Precautionary Intensity corresponds to a design basic acceleration of ground motion of 0.1g (g is the gravitational acceleration). The site type is category II, corresponding to the 3rd group of seismic ground motion. It is classified based on an array of factors, including the thickness of the construction site cover layer and the equivalent shear wave velocity within the soil layer. It is used to reflect the cumulative amplification effect of the ground condition on the bedrock's seismic vibration. In this case, the test site ground primarily consists of gravel soil, with a cover layer thickness of 20.7 m and a soil layer equivalent shear wave velocity of 245 m/s, which make it a category II site according to the regulation of building seismic performance. The floor, roof and wall panels are all based on the newly proposed LPCP. A representative portion of the reference structure was the room located at the intersection of line 2~3 and line A~B at the ground floor of the building, as shown in the shaded part of Fig. 2. The length and height of the wall and the floor in this room are all

3300 mm. The wall thickness is 200 mm, which contains a 100 mm thick thermal insulation sandwich layer and two 50 mm thick concrete surface layers. The floor is 160 mm thick, with the thermal insulation sandwich layer in the middle being 60 mm thick, and the concrete layers on both sides being 50 mm thick. The walls are connected with cast-in-place concrete structural columns, and the walls are connected to the floor using cast-in-place concrete ring beams. The rationale behind this design lies in the fact that the cast-in-place concrete is cheap to make, easy to implement, making it suitable for rural areas with limited economic and construction technology levels.

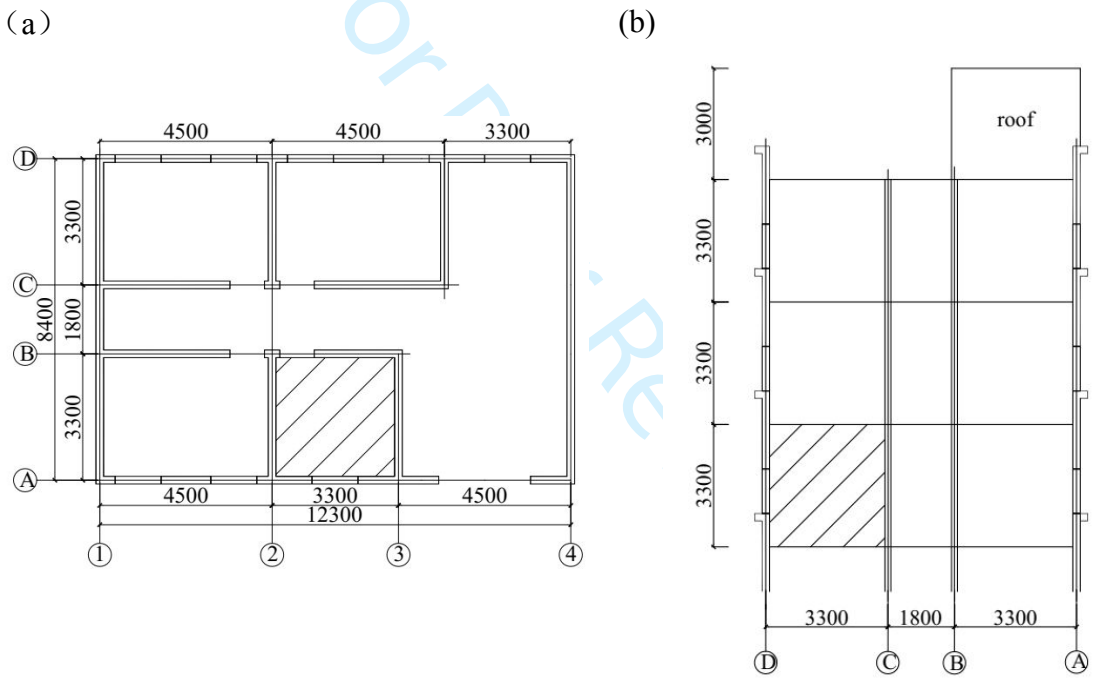

Figure 2. Standard floor layout and cross-section view of building prototype: (a) standard floor layout and (b) crossed-section drawn

2.2*Scaled test specimen*

The test specimen is a 1:2 scale model of the representative portion of the prototype building. The specimen size, material parameters, and loads were calculated using similarity theory (Huang, 2013) and dimensionless analysis are shown in Table 1.

Table 1. Ratio of similitude

Type	Parameters	Similar relation	Scale
Specimen size	Length, L	S_L	1/2
	Area, A	$S_A = S_L^2$	1/4
	Displacement, x	$S_x = S_L$	1/2
	Inertia moment, I	$S_x = S_L^4$	1/16
Material parameters	Elasticity modulus, E	S_E	1
	Poisson ratio, μ	1	
	Strain, ε	1	
	Stress, σ	$S_\sigma = S_E S_\varepsilon$	
	Volume weight, ρ	$S_\rho = S_\sigma / S_L$	
Loads	Earthquake force, F	$S_F = S_E S_L^2$	1/4
	Shear force, V	$S_V = S_E S_L^2$	1/4
	Axial force, N	$S_N = S_E S_L^2$	1/4
	Bending moment, M	$S_F = S_E S_L^3$	1/8

The floor layout and the cross-sectional view of the specimen are shown in Fig. 3. The floor has a plan area of 1670 mm×1670 mm, being 20 mm larger than the room (1650 mm × 1650 mm) to facilitate its connection to the wall. For the sake of simplification, the door and window openings are both located at the centre of the wall.

The dimensions of wall and floor and the associated reinforcement strategy are shown in Fig. 4. The width and height of the wall are both 1650 mm. The wall thickness is 100 mm, with the thermal insulation layer and two concrete layers on both sides being 50 mm and 25 mm thick, respectively. The length and width of the floor are both 1670 mm. The floor thickness is 80 mm, with the thermal insulation layer and concrete surface layers on both sides being 30 mm and 25 mm thick, respectively. A galvanized steel wire mesh with 2 mm diameter steel wire diameter and 200 mm spacing are placed at the centre of concrete layer, which is connected with a set of two-way slanted galvanized steel wires also being 2 mm in diameter and at 200 mm centres.

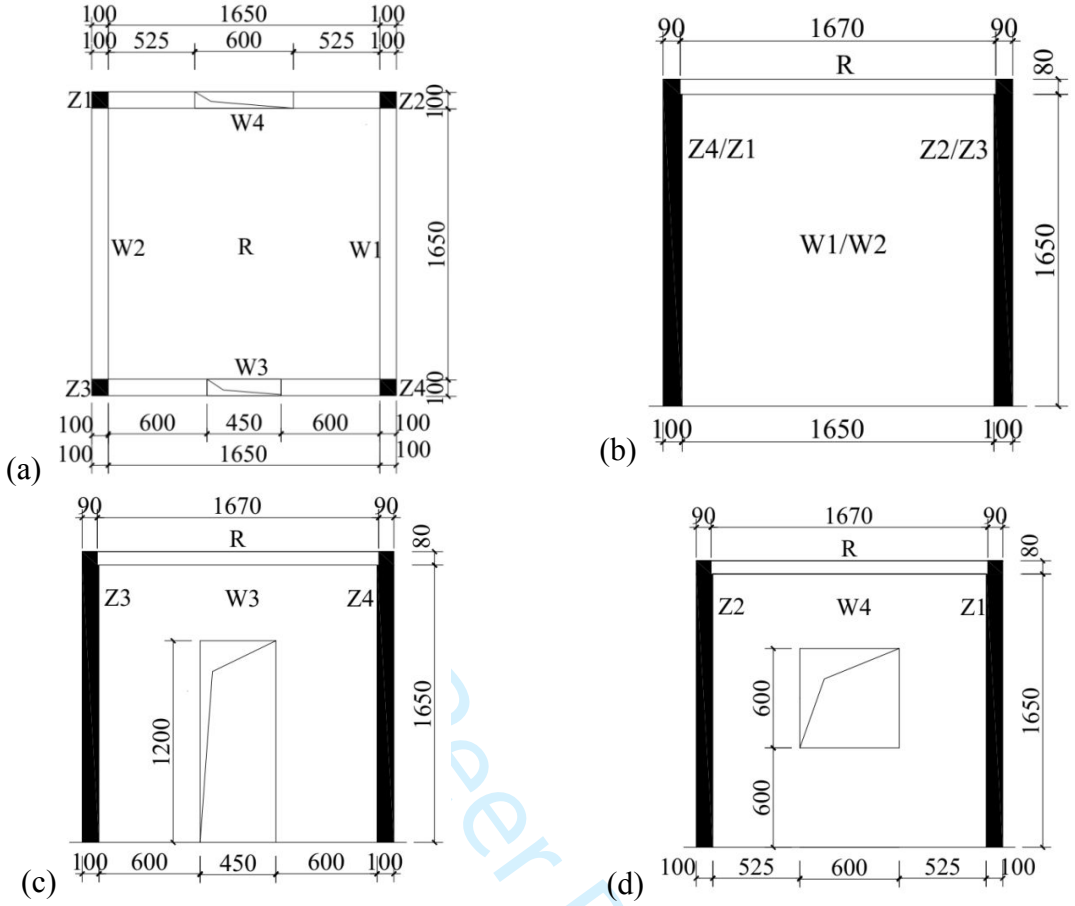

Figure 3. Floor layout and cross-sectional view of the test specimen:(a) Plane figure,(b) Side elevation,(c) Front elevation and (d) Back elevation

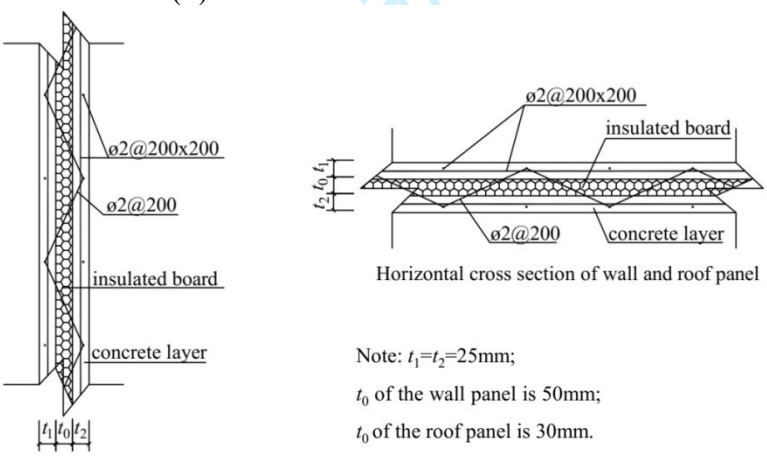

Figure 4. The specimen cross-sectional details

Fig. 5 shows how a wall is connected to other walls, floor and foundation. Inter-wall connection is established based on cast-in-place concrete structural columns being 100 mm by 100 mm. The longitudinal bars are based on four plain round reinforcing bars of 8 mm in

diameter. Stirrups are plain round reinforcing bars are 4 mm in diameter with 75 mm spacing. The connection between wall and floor is through cast-in-place concrete ring beams, with a cross-section of 90 mm by 80 mm. The longitudinal reinforcement consists of four plain round reinforcing bars 6 mm in diameter, transverse reinforcement consists of plain round reinforcing bars 4 mm in diameter with 100 mm spacing. The anchor connection between wall and foundation is established by extending the longitudinal galvanized steel wire in the wall to a height above the foundation by 1/3 of the overall height.

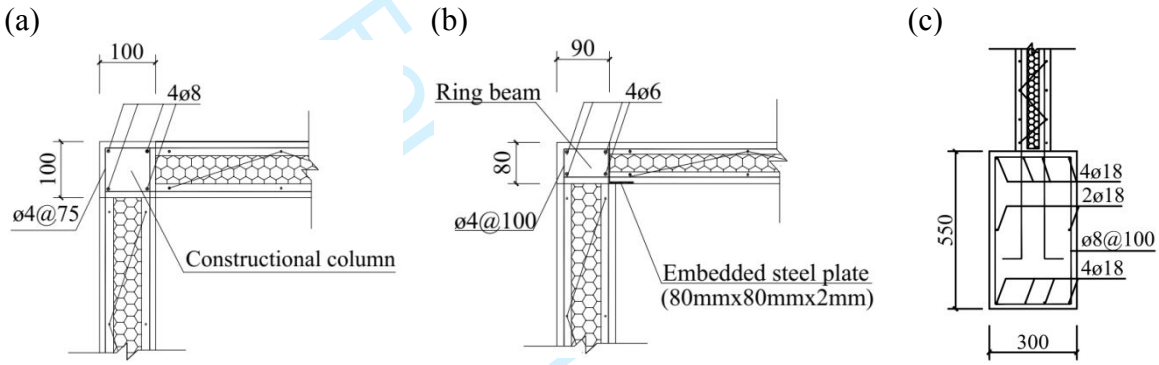

Figure 5. Connection between wall and other walls, floor, and foundation beam: (a) Connection between walls, (b) Connection between wall and roof panel and (c) Connection between wall and foundation beam

2.3 *Materials*

The test specimen mainly consists of concrete and reinforcing bars. The foundation is made of regular concrete with a design strength of 35 MPa, and all the other components are made of fine stone concrete with a design strength of 30MPa.The corresponding compositions are shown in Table 2 and Table 3, respectively. The main purpose of the present testing is to assess the overall seismic performance of the upper building structure as well as the reliability of the connections between components. To prevent the foundation from undergoing damage before the upper structure, the design strength of the foundation concrete is higher than those of the other components. Besides, considering that all the other components except for the foundation

are relatively small, fine stone concrete is used to build those components so as to facilitate the pouring and vibration operations.

The measured concrete strengths are shown in Table 4. The strength measurements were carried out at a factory of prefabricated parts in the city of Leshan. The concrete of all the prefabricated parts are commercially-available self-made concrete produced by the factory, whose actual strength typically exceeds the design value. Table 5 shows the measured strengths of the reinforcing bars.

Table 2. Composition of fine aggregate concrete of 35MPa mix as proportion of cement content

Cement(42.5N)	River sand(0.35~0.5mm)	Gravel（5~31.5 mm）	Water
1	1.11	2.72	0.38

Table 3. Composition of regular aggregate concrete of 30MPa mix as proportion of cement content

Cement(42.5N)	River sand(0.35~0.5mm)	Fine gravel（5~8mm）	Water
1	1.46	3.22	0.52

Table 4. The measured average compressive strength of concrete

Concrete type	Average compressive strength (MPa)	Application
Regular aggregate concrete of C35	53.7	Foundation beam (First concreting)
	51.0	Foundation beam (Second concreting)
Fine aggregate concrete of C30	42.4	Walls, roof panel
	43.4	Structural column, ring beam

Table 5. Mechanical properties of steel bar and zinc-coated wire

Type	Reinforcement diameter	Yield strength (MPa)	Tensile Strength (MPa)
Galvanized steel wire	2mm	392	490
Hot rolled plain steel bars	4mm	401	745
	6mm	506	724
	8mm	545	609

2.4 *Specimen fabrication*

The specimen was prepared through factory prefabrication and field assembly so as to mimic the industrial workflow for constructing buildings with LPCP. The key steps included: setup of

foundation form, binding of foundation reinforcing bars, reservation of structural column reinforcing bars, pouring and curing of foundation concrete (first time), prefabrication of LPCP, installation of LPCP, binding of structural column and ring beam reinforcing bars, pouring and curing of structural column and ring beam concrete, pouring and curing of foundation concrete (second time), and establishment of specimen. The foundation was cast in a two-step process. Initially one third of the foundation height was cast, to fix the reinforcing bars. After the LPCP was in place, the remaining foundation concrete was poured together with the structural column and the ring beam, so as to establish the connection between foundation and the component above it.

3. Testing

3.1 *Test set up*

Both vertical and horizontal loads are applied in the present testing. During the experiment, vertical load is first applied, followed by the application of horizontal load while maintaining a constant vertical load. The vertical load is applied to mimic the load from the top of the room and the live load from the floor. Through calculation, it is determined that the load from the top of the room is 50 kN, while the live load from the floor is 0.5 kN/m^2.

The horizontal load is applied through multiple cycles to model the pattern of reciprocating force and deformation change during an earthquake. The seismic precautionary intensity is set to 7, and the design basic acceleration of ground motion is set to 0.1*g*. Calculation indicates that, with a horizontal earthquake, the ultimate capacity of specimen is predicted to be 220kN. The horizontal load is applied in stepwise cyclic manner toward positive direction. The incremental change of each cycle is set to 1/10 of the predicted ultimate capacity, i.e., starting off from 20kN and adding load in a cyclic stepwise manner until the specimen failure.

3.2 *Loading apparatus*

The specimen is mounted to the ground base slot through four 65 mm diameter 900MP a yield strength anchor bolts. Meanwhile, horizontal supports are set at both sides of the foundation to prevent the foundation from undergoing lateral movement during loading process (Fig. 6).The field picture of loading devices is shown in Fig. 7.

The load transferred from the top of the room was simulated with a vertical servo actuator (maximum force is 2MN). First, 50 kN of concentrated load was applied to a 200 mm by 200 mm by 10 mm steel plate through the vertical servo actuator; the load was in turn propagated to a large steel plate being 1890 mm×1890 mm×20 mm, which converted the concentrated load to a linear load being applied to an I-type steel beam. The I-type beam propagates the load to a ring beam. Four rolling bars 32 mm in diameter were placed between the small steel plate and the large steel plate to ensure that the specimen could move freely within ±100mm during the horizontal loading process. A live load of 0.5 kN/m^2 was applied through gravel uniformly distributed on the floor of the specimen.

The load step was 20kN according to simple calculation. When the specimens cracked, the testing load was controlled by displacement and each load step with an increment of 3.0 times of the crack displacement Δcr. When the wall was completely failed or the loading decreased to 0.85 times the ultimate load, the test stopped. The horizontal load was applied through a horizontal servo actuator (maximum force is 2 MN) mounted to the counter wall. A 600 mm × 300 mm × 20 mm rectangular steel plate was placed at the front of the horizontal servo actuator, which was connected to a 1890 mm×1890 mm×20 mm thick rectangular steel plate at the front of the specimen through four bolts 36 mm in diameter and 500 MPa in yield strength. This configuration allowed the horizontal load to be evenly propagated to the ring beam at the front of the specimen. A ball joint was place in a built-in force sensor in the horizontal servo actuator,

which allowed the horizontal servo actuator to rotate in response to the movement of the specimen so as to ensure the stability of horizontal loading process.

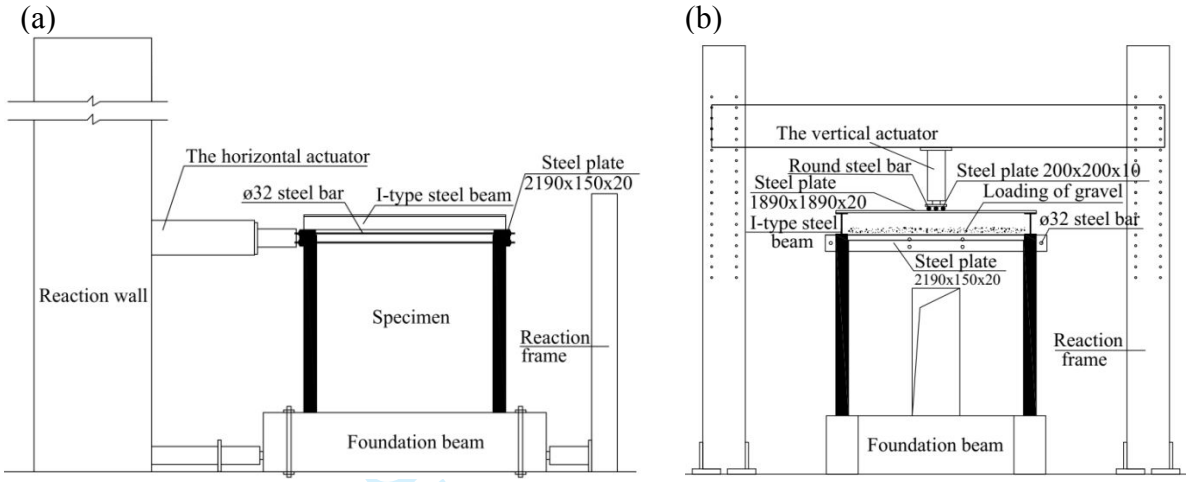

Figure 6. Schematic diagrams of horizontal and vertical loading devices: (a) device for horizontal loading and (b) device for vertical loading

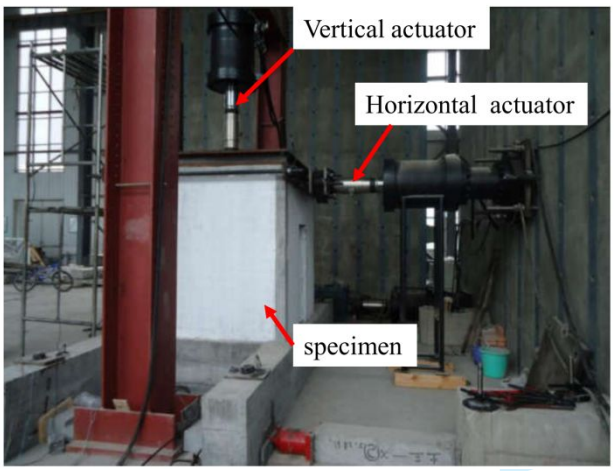

Figure 7. Field picture of loading device

3.3 *Experimental measurement*

The parameters measured during the present testing were: 1)horizontal displacement 2)corresponding lateral load at the top of the specimen and 3)the growth and distribution of cracks in the specimen.

The horizontal displacement at the top of the specimen is measured with a laser displacement sensor located at the centre of the specimen ring beam. Meanwhile, a dial indicator was used to measure the sliding displacement of the foundation at the centre of the

specimen foundation during the loading process so as to eliminate the impact of foundation slippage on the measurement of specimen displacement. The horizontal load was controlled and measured through the control unit of the horizontal servo actuator.

To facilitate the observation of crack growth, a layer of white lime paint was uniformly applied to the surface of the specimen wall, and a 100 mm ×100 mm grid was drawn on the paint using a pencil. During the loading process, a real time observation of the crack initiation, growth, and distribution was conducted, with the shape and direction of the cracks marked out. Evolution of the horizontal load was recorded, and a tape measure and a crack observer are employed to recording the length and width of the crack.

4. Results

4.1 *Ultimate capacity*

The cracking, ultimate, and failure loads of the sample and the corresponding horizontal displacements are shown in Table 6. The cracking load was recorded when the first visible crack appears on the surface of the sample; the ultimate load corresponds to the peak load the sample was able to withstand during the loading process; the failure loads was recorded when the load-bearing capacity of the sample drops to 85% of the ultimate load.

Table 6. Measured horizontal loads and displacements of specimen

Cracking stage		Ultimate stage		Failure stage	
P_{cr} (kN)	Δ_{cr} (mm)	P_{max} (kN)	Δ_{max} (mm)	P_u (kN)	Δ_u (mm)
160	4.39	370	19.97	300	43.48

4.2 *Damage process*

Table 7 shows the damage process of the specimen under the vertical load F_v=50 kN and floor live load q_v=0.5kN/m^2, while the initiation, growth, and distribution of the cracks were shown in Fig. 8.

Table 7. Process of specimen damage

Horizontal load	Damage process	Comments
0-140kN	• Specimen intact; no visible cracking	
160kN	• Fine horizontal cracks appear at the bottom of the structural column Z4	Appearance of the first crack
180 kN	• New fine cracks appear and grow along slanted directions 50 mm above the bottom of the structural column Z4	
200kN	• The width and length of the existing cracks in the structural column Z4 further increase. • Fine horizontal cracks appear at the connection between the wall W1 and the foundation, with the paint on the wall at the connection peeling off slightly.	
220 kN	• A 100 mm long and 0.3 mm wide crack as well as a slanted 80 mm long and 0.3 mm wide crack appear 200 mm above the bottom of the structural column Z4.	
240 kN	The horizontal crack 200 mm above the bottom of the structural column Z4 starts to propagate into the wall W3.	
260 kN	• The horizontal crack reaching the wall W3 starts to grow along a slanted direction toward the bottom of the wall. • A new crack appear 300 mm above the bottom of the structural column Z4	
280 kN	• The horizontal crack reaching the wall W3 finally reaches the bottom of the wall along a slanted direction.	
300 kN	• The length, width, and depth of the existing cracks in the structural column and wall further increase, while an array of new cracks also appear. • A horizontal crack 80 mm long and 0.6 mm wide appears 450 mm above the bottom of the structural column Z4. • The crack at the bottom of the structural column Z4 extends to the wall W1. • A 45^{o} slanted major crack 600 mm long and 0.8 mm wide appears 720 mm above the bottom of the wall W2. • A new crack 600 mm long and 0.8 mm wide appear at the door hole of the wall W3, which first grows along 45^{o} direction, and then grows vertically.	
320kN	• A horizontal crack 100 mm long and 0.5 mm wide appears 500 mm above the bottom of the structural column Z4. • The 45^{o} slanted major crack in the wall W2 continues to extend toward the bottom in an inclined manner; meanwhile, new fine cracks appear at the bottom. • The slanted crack at the door hole of the wall W3 further grows.	
340 kN	• A new slanted crack appears at a location above the bottom of the structural column Z3 by a clearance of 2/3 of the overall column height; the crack grows into the wall W2, with the length and width being 150 mm and 0.4 mm, respectively. • A new horizontal crack 200 mm long and 0.6 mm wide appears on the right hand side 330 mm above the bottom of the wall W3. • The 45^{0} slanted major crack in the wall W2 reaches the bottom of the wall.	
360 kN	• A new slanted crack 100 mm long and 0.5 mm wide appears at a location above the bottom of the structural column Z4 by a clearance of 4/5 of the column height.	
370kN	• The specimen reaches its ultimate capacity, showing significant plastic deformation.	All cracks appear

	• A new horizontal crack 100 mm long and 0.4 mm wide appears 100 mm above the bottom of the structural column Z3. • A horizontal crack 460 mm long and 0.8 mm wide appears 230 mm above the bottom, which then grows into the wall W2. • A multitude of new slanted cracks appear at the door hole of the wall W3. • A slanted crack 200 mm long and 0.4 mm wide appears 500 mm above the bottom; the bottom concrete experiences cracking and detachment.
300 kN	• The load-bearing capacity of specimen starts to decline; a full damage of specimen occurs when the load-bearing capacity reaches 85% of the ultimate capacity (approximately 300 kN). • When the full damage occurs, the concrete at the bottom of the stretched structural columns (Z4、 Z3) experiences severe cracking and detachment; the rebars inside the columns are pulled apart from the foundation; subsequently, the concrete at the bottom of the stretched walls (W3, W2, W1) is cracked, the wall is detached from the foundation, and the vertical rebars are partly snapped.

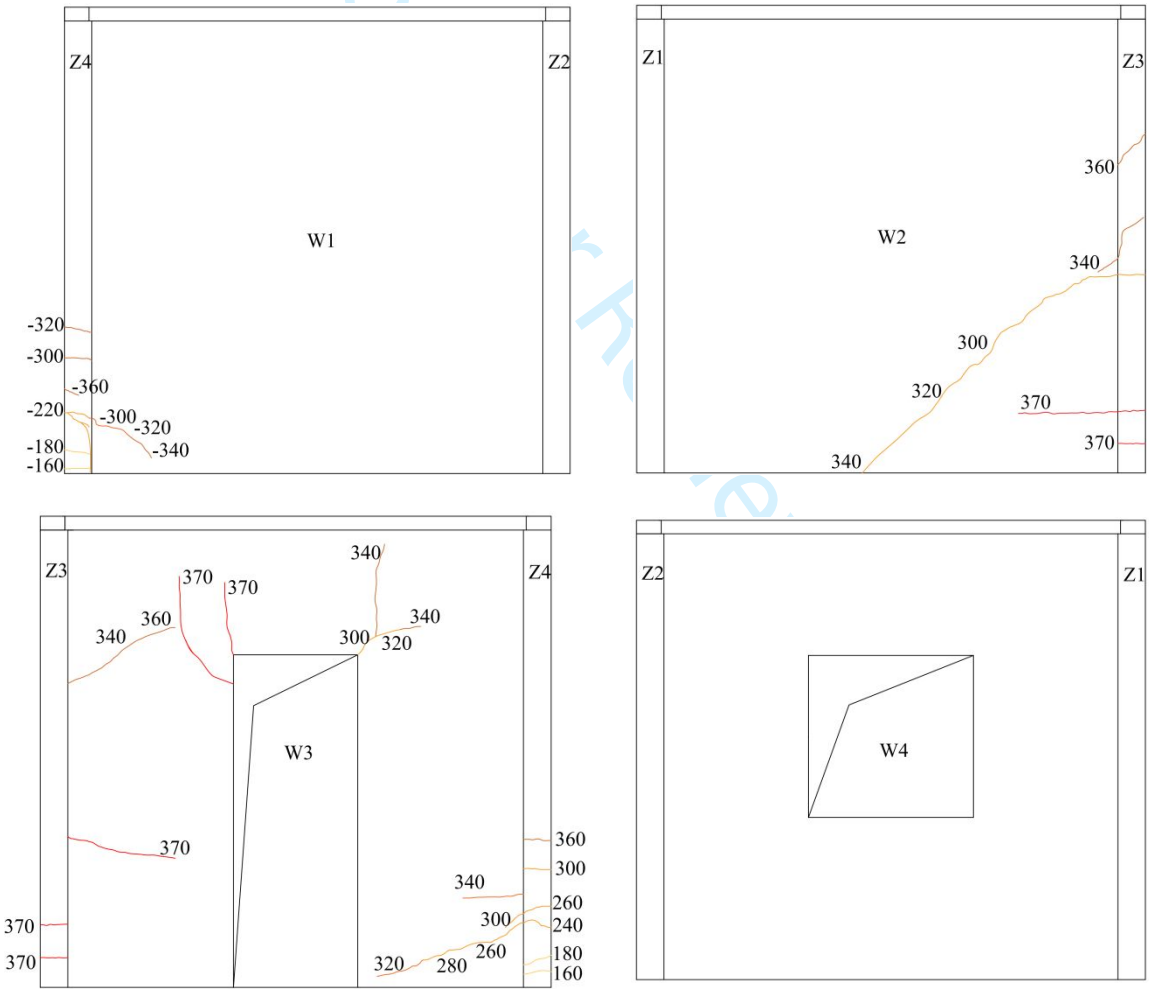

Figure 8. Growth and distribution of cracks of the 4 walls in the specimen

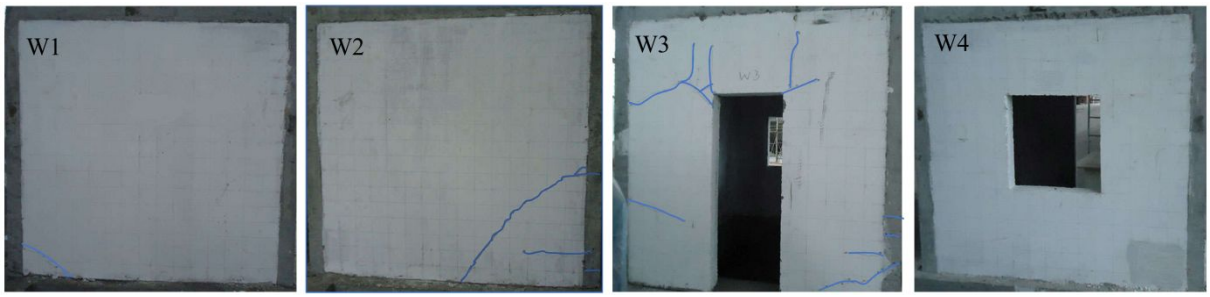

Figure 9. Fully damaged patterns of the 4 walls in the specimen

5. Discussion

5.1 *Ultimate capacity*

The ultimate capacity of specimen is measured to be 370 kN, which is 68% higher than the predicted ultimate capacity (220 kN). It satisfies the required load-bearing capacity, with a large safety margin, indicating that the predicted ultimate capacity is conservative. It is recommended that further study could be maintaining the safety and reducing cost of the wall by decreasing the strength of the concrete to some extent. For instance, the strength of the roof and wall should be reduced from the current 43.4 MPa to 25 ~ 30 MPa, while the foundation's strength could be reduced from the current 53.7 MPa (the 1st pouring) and 51 MPa(the 2nd pouring) to 30 MPa which may lead to cost reduction. The ratio of cracking load to ultimate load is 0.43, while the corresponding ratio of displacements is 0.22, which indicates that the specimen undergoes substantial deformation as it evolves from the cracking stage to the ultimate capacity stage, and a brittle damage is avoided. The specimen's ratio of damage load to ultimate load is 0.81, while the corresponding ratio of displacements is 2.2, which indicates that the specimen still retains its load-bearing capacity and ductility to some extent after the ultimate load is reached.

5.2 *Damage characteristics*

The damage and crack growth processes of the sample are summarized below:

- During damage of the specimen, the overall integrity of the building structure can be maintained, indicating that the building structure assembled based on cast-in-place

concrete structural columns and ring beams exhibits a decent level of structural robustness.

- The final damage of specimen is found to be as follows: the concrete at the bottom of the structural column (Z1, Z2) on the loading side undergoes a marked cracking, with the reinforcing bars on the loading side within the column pulled apart. Subsequently, the walls on the loading side (W1, W2, W3) gradually detach from the foundation, the galvanized steel wires in the walls are pulled apart, with the specimen's load-bearing capacity dropping to 85% of the ultimate capacity, which signifies the occurrence of full damage. Therefore, one needs to reinforce the connections among foundation, structural columns, and walls during the design.
- With the presence of both horizontal stepwise cyclic loading toward positive direction and the vertical loading, most cracks are inclined, being located at the middle and bottom sections of the wall as well as the opening on the loading side. This pattern indicates that the middle and bottom sections of the wall and the opening are the main load-bearing locations and the weak part of the whole structure. As such, these locations need to be reinforced during the design. Meanwhile, it is found that the growth of cracks in the wall is uneven and inadequate. To further improve the wall's energy-dissipating ability, one needs to optimize the building structure based on LPCP.
- The thermal insulation sandwich layer is not detached from the concrete layers on both sides, indicating that the various components of LPCP can function in a concerted manner, and the wallboard shows a decent overall integrity.
- From the initial loading to the final damage, the specimen roughly undergoes five stages, namely elastic stage, cracking stage, yield stage, limit stage, and damage stage, which shows that the specimen undergoes significant change before the final damage, exhibiting a good ductility.

5.3*Hysteresis curve and skeleton curve*

Fig. 10(a) shows the load-displacement curve (hysteresis curve) obtained from the simulated earthquake-induced cyclic loading. It can be seen in Fig. 10(a) that during the initial loading, the load-displacement curve is roughly linear, while the residual deformation is insignificant, i.e., the specimen is in elastic regime. As the horizontal load reaches 160 kN, cracks start to appear in the specimen, and residual deformation occurs. As a result, the load-displacement curve is transformed from a linear curve to a loop curve, i.e., a hysteresis loop appears. This indicates that the specimen starts to dissipate the earthquake energy. With an increase of load, the number of cracks in the specimen keeps increasing, the residual deformation becomes increasingly pronounced, the area covered by the hysteresis loop gradually ramps up, and the hysteresis loop starts to exhibit a reversed S shape. A combination of these observations indicates that the specimen's dissipation of seismic energy increases gradually, and slippage occurs. As the ultimate load 370 kN is reached, the specimen's load-bearing capacity starts go down, the area of hysteresis loop further increases, and the slippage becomes more pronounced. This trend continues to progress until the load-bearing capacity drops to 85% of the ultimate capacity, a point marking the occurrence of full damage. It can be observed from the hysteresis curve that the earthquake-induced deformation characteristics and energy dissipation processes associated with the building structure based on LPCP highly resembles that of the shear wall structure with reinforcing bar concrete. Therefore, one can refer to the shear wall structure with reinforcing bar concrete for earthquake resistant design.

By drawing an envelope curve passing through the peak of each load hysteresis curve as derived from the cyclic loading process, one can obtain the skeleton curve of the specimen, as shown in Fig. 10 (b). Before cracks in the specimen appear, the skeleton curve is almost linear, corresponding to a large structural stiffness and the elastic state. As the cracks start to appear,

the slope of the curve starts to decline, i.e., the specimen's horizontal displacement gradually increases for a given incremental load. As the ultimate load is reached, the specimen's load-bearing capacity starts to drop all the way to 85% of the ultimate capacity, marking the occurrence of full damage. The decline curve is relatively shallow, indicating that the specimen, after the ultimate capacity is reached, still retains a portion of its load-bearing capacity and ductility.

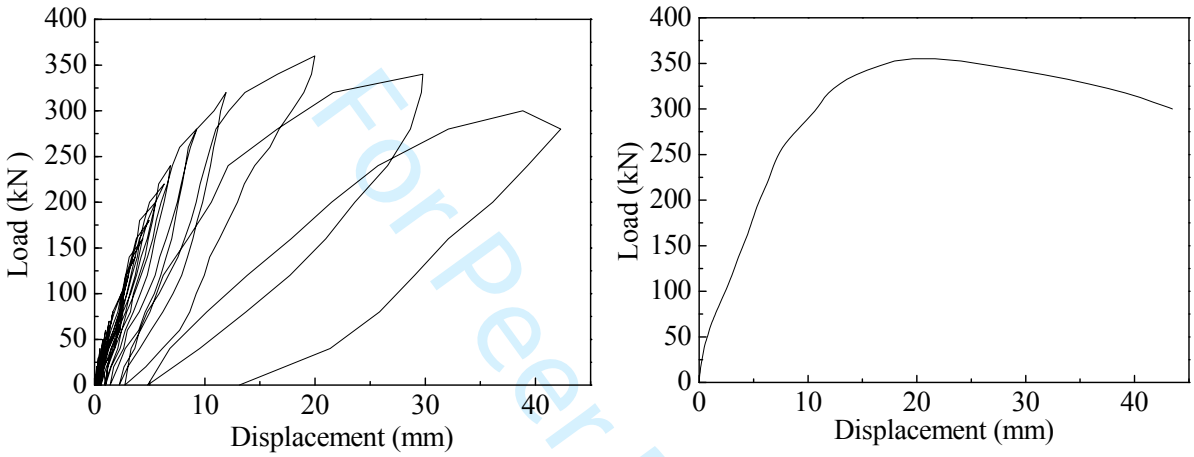

Figure 10. Hysteresis curve and hysteretic skeleton curve of specimen: (a) hysteresis curve and (b)hysteretic skeleton curve

5.4*Stiffness degradation curve*

The specimen's stiffness degradation curve is shown in Fig. 11. The specimen's stiffness degradation process mainly consists of three stages: 1) Rapid decrease of stiffness stage, which corresponds to the process from the point with initial appearance of fine cracks in the concrete to the point with apparent cracks visible to naked eyes; the increase of displacement during this stage is relatively small, while the drop of stiffness is substantial (71%), i.e., from 142.86 kN/mm to 41.42 kN/mm. 2) Moderate decrease of stiffness stage, which corresponds to the point where the specimen undergoes cracking to the point where the ultimate capacity is reached; during this stage the decrease of stiffness becomes much smaller, i.e., from 41.42 kN/mm to 18.03 kN/mm, a 12.6% decrease. (3) Slow decrease of stiffness stage, which corresponds to the point where the ultimate capacity is reached to the point where the full

damage occurs; during this stage, the displacement is substantially raised, whereas the decrease of stiffness is small, i.e., from 18.03 kN/mm to 6.90 kN/mm, a 7.8% decrease.

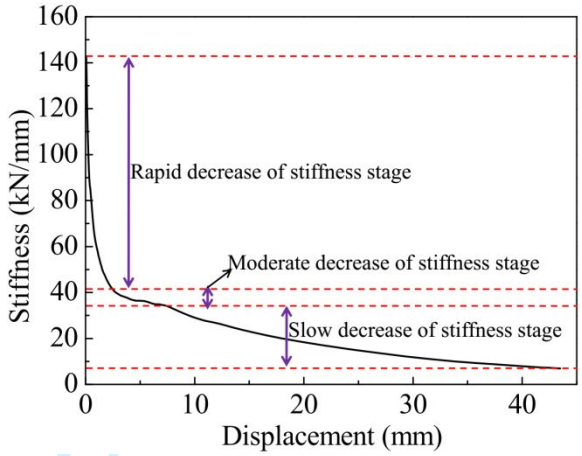

Figure 11. Stiffness degradation curve of specimen

5.5*Ductility factor*

The ductility factor μ denotes the ratio of maximum displacement Δ_u to the yield displacement Δ_y when specimen damage occurs, and is used here to assess the structural ductility. Due to the absence of an apparent yield point on the specimen's skeleton curve (Fig. 10(b)), one can use the Generalized Yield Moment Method(GYMM) to determine the yield point.(Liu, 2007; Huang et al, 2018). Fig. 12 outlines the key steps of this method: draw a tangential line *OH* going through the origin *O*, and draw a horizontal line that passes through the peak load at *G*; suppose these two lines intersect each other at point *H*; draw a perpendicular line through *H*, which intersects the skeleton curve at *I*; extend the line *OI* to cross the line *HG* at point *H'*; draw a perpendicular line through *H'*, which intersects the skeleton curve at point *B*, which is a decent approximation of the yield point. The yield load and displacement obtained from the aforementioned GYMM was 280 kN and 9.25 mm, respectively. And the maximum displacement was 43.48mmas showed in Table 6.It is found through calculation that the specimen's ductility factor is 4.7 according to dived the maximum displacement by the yield displacement, which satisfies the seismic regulation dictating that the concrete structural

ductility factor should exceed 3. This indicates that the building structure based on LPCP has decent ductility.

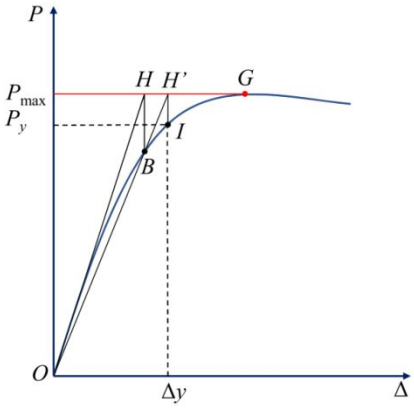

Figure 12. Schematic diagram of Generalized Yield Moment Method

5.6 *Energy-dissipating ability*

The specimen's energy-dissipating ability can be analysed based on working index, which can be calculated using Eq. (1):

$$I_{\mathrm{W}}^{\mathrm{S}} = \frac{\sum_{i=1}^{n} P_i \Delta_i}{P_y \Delta_y} \tag{1}$$

Where P_{i} and Δ_i denote the peak load value and the corresponding displacement for the *i*th cyclic loading; P_{y} and Δ_{y} denote the yield load and displacement values, respectively(Jiang et al, 2007;Huang, 2013). It is found through calculation that the specimen's working index is 20.62, which is much larger that these of other composite wallboard structures, e.g., the fibre gypsum board composite wall filled with concrete with a working index of 7 to 8. One can thereby conclude that the newly proposed building structure based on LPCP can deliver a strong energy-dissipating effect.

6. Conclusions

This study investigated the overall seismic performance of the LPCP building structure which formed by the connection of cast-in-place concrete ring beam and column based on the results of the previous studies, and obtained the conclusions as follow:

1. The structure has a high load-bearing capacity, decent ductility, and strong energy-dissipating ability, allowing it satisfy the seismic performance requirements concerning China's rural building structure. Meanwhile, the construction workflow based on factory prefabrication and field assembly is conductive to energy conservation, making this technology particularly promising.

2. The present building structure assembled based on cast-in-place concrete structural columns and ring beams exhibit good structural robustness. Meanwhile, during the loading process, various components in the LPCP can function in a concerted manner, the wall panel has strong integrity.

3. The middle and lower sections of the wall and its connection with the foundation are the key load-bearing location and the weak part of the entire structure. Hence, it is recommended to reinforce these places during the design.

7. Future work

1. The prefabricated concrete wall panels currently suffers from a series of issues, incuding the large size and weight,a stringent requirement on the transportation and installation, and high sensitivity to the rural areas road condition, transportation vehicles, mechanical equipment and construction technology. Future research needs to focus on reducing the weight and size of the LPCP so as to faciliate the transportation in the rural area.

2.The interconncetion of LPCP parts is critical for ensuring the seismic performance of the overall building structure. Hence, future research will study the impact of various interconnection methods on the seismic performance of the LPCP building structures so as to meet the relevant regulations in the rural area.

3. The stepwise cyclic loading toward positive direction used in the present experiments cannot authentically mimic the actual earthquake condition. It is thereby advised to conduct improved seismic performance experiments if possible that can more authentically reflect the impact of earthquake, e.g., shaking table test.

Acknowledgements

The author would like to thank for the financial sponsorship of Southwest Jiaotong University, which provided the first fund to open this research subject (Grant No. 10101X10096060). This project has also been supported financially also by Project of Young Scientists Fund (Grant No. 51808454, 51508472), Science and Technology Innovation Project of the Fundamental Research Funds for the Central Universities (Grant No.10101B10096033) and Science and Technology Citizen-Benefiting Project of Chengdu City (Grant No. 2015-HM01-00063-SF).

Statement

The Author(s) declare(s) that there is no conflict of interest.

References

Bai J , Cheng F, Jin S, Ou J(2019) Assessing and Quantifying the earthquake response of reinforced concrete buckling-restrained brace frame structures. *Bulletin of Earthquake Engineering*, 17:3847-3871.

Benayoune A, Abdul A and Samad A (2008) Flexural behaviour of pre-cast concrete sandwich wallboard-Experimental and theoretical investigations. *Construction and Building Materials*, 22(1):580-592.

Benayoune A, Samad A AA, Ali A AA and Trikha D N (2007) Response of pre-cast reinforced composite sandwich panels to axial loading. *Construction and Building Materials*, 21(5): 677-685.

Benayoune A, Samad A A Abdul, Trikha D N, Ali A A A and Ashrabov A A (2006) Structural behavior of eccentrically loaded precast sandwich panels. *Construction and Building Materials*, 20(1): 713-724.

Cao W, Zhang Y and Dong H (2015) Research and application on seismic energy-saving structural system for rural buildings. *Engineering Mechanics*, 32(12):1-12.

Huang Q (2013) *Research on seismic and energy-saving performance of new type 3D –building in rural area*. Ph.D. thesis, Sichuan University, China.

Huang Q, Liang D, Huang Y and Rui Y (2018) Numerical analysis on seismic performance of loadbearing 3Dwalls. *Journal of Southwest Jiaotong University*,53 (5):983-988.

Huang Q, Xiong F and Zhou N(2014) Experimental research on seismic performance of new type 3D-walls. *Journal of Sichuan University,*46(3):15-22.

Isabella G, Matteo C and Marcodi P (2015) Bending behaviour of Textile Reinforced Concrete sandwich beams. *Construction and Building Materials,*95: 675-685.

Janardhana M, Davis P R, Ravichandran S S, Prasad A M and Menon D. (2014) Calibration of a hysteretic model for glass fiber reinforced gypsum wall panels. *Earthquake Engineering and Engineering Vibration*, 13(2): 347-355.

Ji G. (2018) The economic and feasibility analysis of gas and coal were used as fuel for making sintered brick. *Tile*, (8):40-44.

Jia H, Zhang D, Zheng S Xie W and Pandey M D (2013) Local site effect on a high-pier railway bridge under tridirectional spatial excitations: nonstationary stochastic analysis. *Soil Dynamics and Earthquake Engineering*, 52:55-69.

Jiang X, Gu Y (2007) Restoring-Force Test of Fiber-Reinforced Plasterboard with Concrete Core Column. *Journal of Tianjin University*,40(5):542-547.

Kabir M (2005) Structural performance of 3D sandwich wallboards under shear and flexural loading. *Scientia Iranica*,12(1):402-408.

Liu K. (2013) Shear Strength of Concrete and Gypsum Composite Walls. *Applied Mechanics and Materials*, (368-370): 976-983.

Liu Y(2007) *An experimental study on seismic behavior of CS wallboard structure*, Master thesis, Tianjin University, China.

Magliulo G, Petrone C, Capozzi V, Maddaloni G, Lopez P, Manfredi G. (2014) Seismic performance evaluation of plasterboard partitions via shake table tests. *Bulletin of Earthquake Engineering*, 12: 1657-1677.

Mohamad N and Hassan N (2013) The structural performance of precast lightweight foam concrete sandwich panel with single and double shear truss connectors subjected to axial load. *Advanced Materials Research*, 638(1): 2746-2751.

Mohamad N, Mahdi and Muhammad H. (2011) Testing of precast lightweight foamed concrete sandwich panel with single and double symmetrical shear truss connectors under eccentric loading. *Advanced Materials Research*, 336(2): 1107-1116.

National standard of the People's Republic of China: GB50011-2010 (2010) Code for design of buildings.

Ramachandra M V, Ramesh K and Smitha G (2014) Structural performance of precast and cast-in-situ ultra high strength concrete sandwich panel. *Tech Science Press CMC*44(1):59-72.

Retamales R, Davies R, Mosqueda G and Filiatrault A (2013) Experimental seismic fragility of cold-formed steel framed gypsum partition walls. *Journal of Structural Engineering*, 139: 1285-1293.

Rodrigo L, Joaquim B, Isabel B and Miguel A (2013) Development of sandwich panels combining fibre reinforced concrete layers and fibre reinforced polymer connectors. Part I: conception and pull-out tests. *Composite Structures*, 105(8): 446-459.

Smitha G V, Ramesh K and Harishkumar S (2014) Pre-fabricated sandwich panels using cold-formed steel and textile reinforced concrete. *Construction and Building Materials*, 64: 54-59.

Tian J and Su J (2006)The basic measures to mitigate earthquake disaster in rural area. *Construction Quality*(11):15-17.

Waiel M and Faruk K (2009) Behavior of single-story lightweight panel building under lateral loads. *Journal of earthquake engineering*13(1):100-107.

Wang Y(2015) *Whole life cycle carbon emissions research of industrialized precast construction*. Ph.D. thesis, Southeast University, China.

Wu Y F and Dare M P (2006) Flexural and shear strength of composite lintels in glass fiber reinforced gypsum wall constructions. *Journal of Materials in Civil Engineering*, 18: 415-423.